Multichannel Differential Group Delay Emulation and Compensation via a Phase Pulse Shaper

Shawn X. Wang, *Student Member, IEEE*, and Andrew M. Weiner, *Fellow, IEEE*

***Abstract*—We developed a differential group delay (DGD) emulator which is based on a high spectral resolution phase pulse shaper. DGD generation has been demonstrated for up to four wavelength channels independently and simultaneously, with DGD accuracy of approximately 1 ps for up to 400-ps DGD range. For each channel, DGD versus frequency profiles can be arbitrarily programmed to user specifications. Multichannel DGD compensation has also been demonstrated using the same setup.**

***Index Terms*—Fiber characterization, optical fiber communications, polarization-mode dispersion (PMD), pulse shaping.**

I. Introduction

POLARIZATION-MODE dispersion (PMD) is a major performance limiting factor in pushing long-haul lightwave communication systems beyond 10 Gb/s. PMD can be described by the PMD vector $\mathbf{\Omega}(\omega)$, with its direction defining the fiber's principal states of polarization (PSP) and its magnitude defining the differential group delay (DGD). Due to the statistically time-varying nature of PMD within a fiber, a PMD emulator is often utilized for characterizing PMD and PMD-induced system penalties by cycling through the various PMD states expected in an optical fiber. While statistical tunability of the produced DGD has been reported using current emulator designs based on the concept of a series of birefringent elements with independently tunable DGDs [1], [2], deterministically generating the exact frequency-dependent DGD profile desired by the user may be difficult. With deterministic controllability of the DGD emulator, techniques such as importance sampling can be applied to more efficiently study PMD effects involving low probability events of large DGD, for which higher order (frequency dependent) PMD terms become increasingly pronounced. We have recently reported on a DGD emulation technique based on a phase pulse shaper [3] which is capable of applying arbitrary user-defined DGD versus frequency profiles to a wavelength-division-multiplexing (WDM) channel under test. However, a key challenge in PMD research is to find WDM implementations that allow multiple wavelength channels to share a single compensator, sensor, or emulator device. In a typical PMD emulator where all-optical channels are fed through the same optical elements, the DGD statistics of different channels cannot be independently controlled. A device capable of independent multichannel control would contribute to substantial cost and practicality advantage compared to dedicating one unit for each channel.

A multichannel chromatic dispersion slope compensator based on a pulse shaping scheme with a fixed phase mask was demonstrated in [4]. Here we extend our high spectral-resolution Fourier pulse-shaper-based DGD emulator to generate essentially arbitrary DGD versus frequency profiles for four wavelength channels simultaneously and independently. First-order PMD range has been tested up to ± 400 ps with an accuracy of approximately 1 ps, and higher order DGD profiles produced have demonstrated excellent agreement with theoretical simulations. In addition, we have also demonstrated the pulse shaper as a first-order PMD compensator for multiple channels experiencing different amounts of DGD. This work suggests that other optical signal processing operations based on programmable pulse shaping, including tunable dispersion compensation, wavelength-parallel polarization control, and all-order PMD compensation [5]–[7], can also be extended to independent multiwavelength-channel configurations.

II. Theory

The Jones Matrix describing a birefringent element is

$$T(\omega) = e^{-j\Psi(\omega)} \begin{bmatrix} e^{j\phi(\omega)} & 0 \\ 0 & e^{-j\phi(\omega)} \end{bmatrix} \tag{1}$$

where $\Psi(\omega)$ is the common-mode phase and $2\phi(\omega)$ is the phase difference introduced by the two axes of the medium. In our experiment, only differential phase is of interest, therefore $\Psi(\omega)$ is set to zero. By controlling the spectral phase $\phi(\omega)$, one can control the group delays $\tau^+(\omega)$ and $\tau^-(\omega)$ of the slow and fast PSP axes through the relation $\tau^-(\omega) = -\tau^+(\omega) = d\phi(\omega)/d\omega$. The DGD is the group delay difference between the slow and the fast PSP axes and can be controlled through the relation

$$\Delta\tau(\omega) = \tau^+(\omega) - \tau^-(\omega) = \frac{-2d\phi(\omega)}{d(\omega)}. \tag{2}$$

By controlling the phase to have desired nonlinear frequency variation, one can generate higher order DGD profiles, defined in a Taylor series about the center frequency ω_0 as

$$\Delta\tau(\omega) = 2\tau + 2\tau_\omega(\omega - \omega_0) + \tau_{\omega\omega}(\omega - \omega_0)^2 + \cdots. \tag{3}$$

Here 2τ is the first-order PMD (constant DGD), and the additional terms represent higher order DGD, respectively. Thus, we use the term DGD here to denote any frequency-dependent delay that is equal but opposite when tested with either of two fixed orthogonal polarization states. In Section III, we describe a multichannel DGD emulator which operates via control of the

Manuscript received February 28, 2007; revised May 6, 2007. This work was supported in part by the National Science Foundation under Grant 0501366-ECS.

The authors are with the School of Electrical and Computer Engineering, Purdue University, West Lafayette, IN 47907-1285 USA (e-mail: wang7@ecn.purdue.edu; amw@ecn.purdue.edu).

Digital Object Identifier 10.1109/LPT.2007.901699

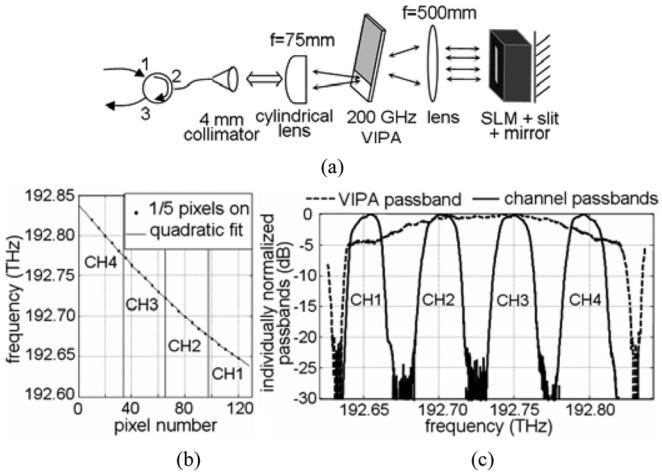

Fig. 1. (a) Schematic diagram of the DGD emulator. (b) Passbands of the VIPA and the four channels under test. (c) Pixel to wavelength mapping.

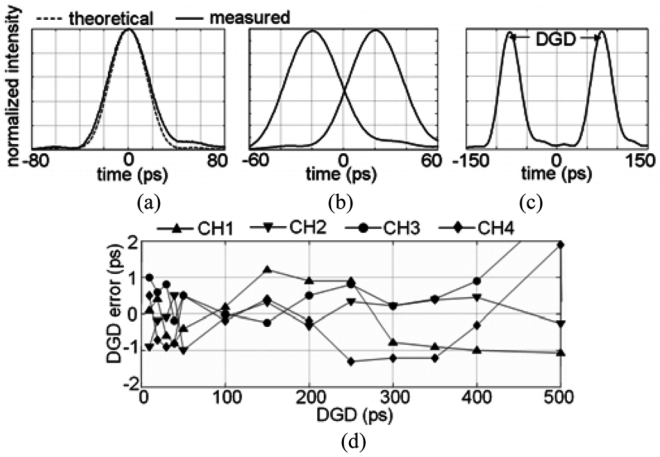

Fig. 2. (a) DGD $= 0$ ps. (b) DGD $= 40$ ps. (c) DGD $= 150$ ps. (d) DGD accuracy for generated DGD range of up to 500 ps.

spectral phase. Our DGD emulator has fixed PSP but can be programmed to generate essentially any user-defined frequency-dependent $\Delta\tau(\omega)$ profile, independently for each of four wavelength channels. By adding spectral polarization control [5], [7] in the future, it should be feasible to achieve multiwavelength control of the full frequency-dependent PMD (both DGD and PSP).

III. Experimental Setup and Results

Fig. 1(a) shows the schematic of a high spectral resolution, Fourier phase pulse shaper [8]. The three main components of the pulse shaper included a circulator, a 200-GHz free-spectral-range (FSR) virtually imaged phased array (VIPA) [9], [10], and a dual-layer 128-element liquid crystal spatial light modulator (SLM). The input light was spectrally dispersed using the VIPA onto the SLM, which ran in a double-pass scheme with a mirror. Due to multiple orders of diffraction of the VIPA, a slit is used in front of the SLM to allow only the dominant order to pass. The total insertion loss of the setup was measured at 12 dB. The 3-dB spectral resolution at the SLM plane is roughly 1.35 GHz, and the frequency spacing between SLM pixels varies from $\sim$2 GHz/pixel for Pixel 1 to $\sim$1.1 GHz/pixel for Pixel 128. This variation in frequency spacing is due to the nonlinear angular dispersion of the VIPA [10], which is illustrated by the quadratic frequency versus pixel mapping in Fig. 1(b). The mapping curve is important for correcting the nonlinear frequency allocation at the SLM plane and was obtained by measuring the output spectrum when every fifth pixel was programmed for transmission, then plotting the peaks in the final spectrum against their respective pixel numbers. A VIPA with larger FSR can be used to cover more WDM channels, but at the cost of worsened spectral resolution [10]. The optic axes of the two layers of the SLM were, respectively, 45° and 135°, with each layer controlling the phase profile of the field polarized along that direction as described in (1). When differential phase is applied to the two orthogonal optic axes, two orthogonal PSP are defined, and DGD between the two PSP can be controlled according to (2). The group delay of each PSP comes from the frequency variation of phase introduced by the SLM. The desired phase profile is programmed onto the SLM modulo 2π (so a maximum phase swing of only 2π per pixel is required). The 200-GHz FSR of the VIPA allows the pulse shaper to cover four adjacent channels on the ITU grid spaced by 50 GHz. In software, we organize the pixels into four different groups that can be programmed independently. This allows frequency-dependent DGD profiles to be independently programmed for each wavelength channel.

The source used for testing the emulator was a mode-locked laser, which was filtered to reduce the bandwidth down to $\sim$20 GHz. The 20-GHz filter was constructed using a diffraction grating pulse shaper with a slit and could be tuned to select each of the four wavelength channels of interest. Fig. 1(c) shows the passbands of the four channels selected from 192.65 to 192.8 THz, each normalized to its own peak value. The pixels dedicated to control the phase profile of each channel are shown in Fig. 1(b). For each channel, the resultant time-domain pulse was roughly 40 ps which resembles a single bit in a 10-G return-to-zero system. Our experiments used a fast photodetector and sampling oscilloscope to directly observe waveform distortions emerged from the programmed DGD.

First, various amounts of constant DGD were generated simultaneously for each of the channels to check the accuracy of the device. Fig. 2(a)–(c) shows sample traces taken from Channel 1. When no DGD is applied to the emulator, the measured pulse agrees with the theoretically simulated pulse, which is the Fourier transform of the spectrum obtained by an optical spectrum analyzer. For DGD less than 100 ps, the pulses split between the fast and slow axes remained partially overlapped, and the measurements were taken for each of the axes separately by polarization controlling all of the pulse energy onto one axis at a time at the input of the DGD emulator. The measured pulses are plotted together on the same time scale in Fig. 2(b), and the DGD is the time difference between their peaks. For DGD greater than 100 ps [Fig. 2(c)], the pulse peaks are well defined, and the pulse energy was split equally onto each of the axes, again by adjusting the polarization controller in front of the DGD emulator. Various amounts of DGD were tested for each of the four channels. As can be seen from Fig. 2(d), the errors were less than 1.2 ps for DGD generation of up to 400 ps. The stability and repeatability of the device were observed to fall within the error margin.

To show the independent programmability of frequency-dependent DGD profiles for each channel, we generated various

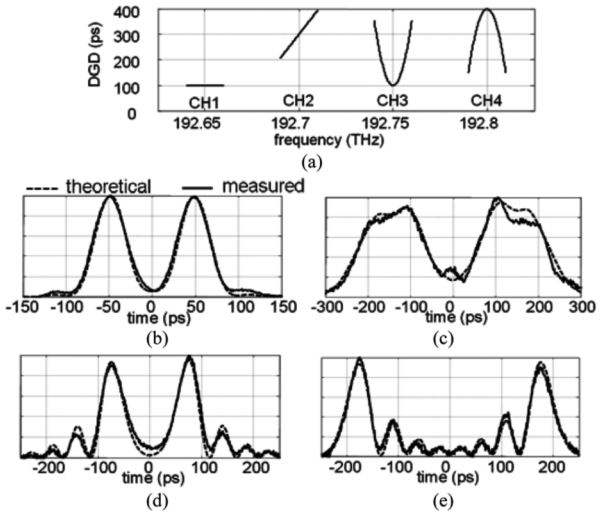

Fig. 3. (a) DGD versus frequency applied to the four channels. (b) Ch1: constant DGD; $\tau = 50$ ps. (c) Ch2: linear DGD; $\tau = 150$ ps, $\tau_\omega = 27.5$ ps^2. (d) Ch3: quadratic DGD; $\tau = 50$ ps, $\tau_{\omega\omega} = 40$ ps^3. (e) Ch4: quadratic DGD; $\tau = 200$ ps, $\tau_{\omega\omega} = -40$ ps^3.

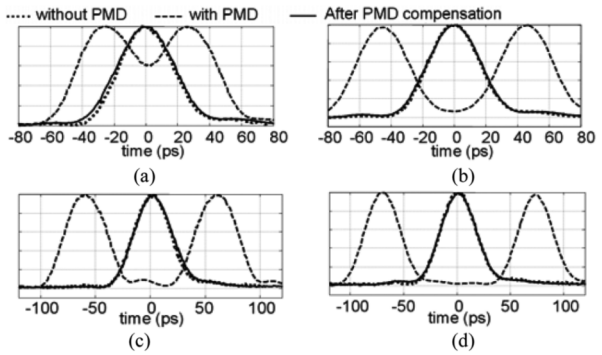

Fig. 4. First-order PMD compensation for (a) Ch1: 51 ps, (b) Ch2: 92 ps, (c) Ch3: 114 ps, (d) Ch4: 143 ps.

DGD profiles onto each of the channels as shown in Fig. 3(a): constant DGD for Channel 1, linear DGD profile for Channel 2, and concave and convex quadratic DGD profiles for Channels 3 and 4. The measured waveforms are compared with theoretical simulations, which are Fourier transforms of the channel spectra with appropriately applied phase profiles. As can be seen from Fig. 3(b)–(e), the measured results agreed very well with the theoretical results. The linear DGD in Channel 2 is a polarization-dependent chromatic dispersion which caused each pulse to broaden, and the quadratic DGD in Channels 3 and 4 have cubic phase which caused the tails in the pulses, all as expected.

The same pulse shaper can also be used to perform multichannel first-order PMD compensation. To show this, we used various lengths of polarization-maintaining fibers to apply different amounts of DGD to each of the four channels under test. The amounts of DGDs applied to Channels 1 through 4 were, respectively, 51, 92, 114, and 143 ps. Ideally, the PMD distorted channels should be simultaneously compensated by first demultiplexing the channels and polarization-control each one independently so that the slow axis of the PM fiber for each channel is aligned with the fast axis of the PMD compensator. This could be accomplished by using a wavelength-parallel polarization controller based on a pulse shaper configuration, as in [5]. However, in this proof of concept experiment, we utilize our existing setup to compensate for PMD in each channel individually. The DGD of the PM fiber was first obtained by measuring the time difference between the output pulses. Then the output of the PM fiber was fed through the pulse shaper with polarization axes aligned manually using a polarization controller. Finally, the proper amount of DGD was manually programmed to the pulse shaper to compensate the PMD of the PM fiber. To automate the compensation process, a feedback signal such as eye diagram, degree of polarization, or spectral polarization would be needed to control both the polarization alignment and the amount of DGD to apply. Fig. 4 shows pulse shapes of each channel before and after PMD compensation, as well as the original pulses without PMD. As expected, the PMD of each channel were successfully compensated.

IV. Conclusion

We have demonstrated a programmable DGD emulator capable of generating arbitrary frequency-dependent DGD profiles for multiple optical channels independently and simultaneously. This emulator could be programmed with algorithms to run user specified DGD evolution for systems testing of PMD tolerance and to characterize outage probability, as well as implementing techniques such as importance sampling with user-defined DGD statistics. The versatility of the device also allowed successful demonstration of multichannel first-order PMD compensation.

Acknowledgment

The authors gratefully acknowledge Z. Jiang for his pulse shaper setup which was used as the 20-GHz bandpass filter, and the donation of the VIPA from C. Lin of Avanex Corporation.

References

[1] L. Yan, M. C. Hauer, Y. Shi, X. S. Yao, P. Ebrahimi, Y. Wang, A. E. Willner, and W. L. Kath, "Polarization-mode dispersion emulator using variable differential-group-delay (DGD) elements and its use for experimental importance sampling," *J. Lightw. Technol.*, vol. 22, no. 4, pp. 1051–1058, Apr. 2004.

[2] L. Yan, C. Yeh, G. Yang, L. Lin, Z. Chen, Y. Q. Shi, A. E. Willner, and X. S. Yao, "Programmable group delay module using polarization switching," *J. Lightw. Technol.*, vol. 21, no. 7, pp. 1676–1684, Jul. 2003.

[3] S. X. Wang and A. M. Weiner, "Fourier pulse-shaper-based high-order DGD emulator," *Opt. Express*, vol. 15, pp. 2127–2138, 2007.

[4] H. Takenouchi, T. Ishii, and T. Goh, "8 THz bandwidth dispersion-slope compensator module for multiband 40 Gbit/s WDM transmission systems using an AWGs and spatial phase filter," *Electron. Lett.*, vol. 37, pp. 777–778, 2001.

[5] M. Akbulut, R. Nelson, A. M. Weiner, P. Cronin, and P. J. Miller, "Broadband polarization correction with programmable liquid-crystal modulator arrays," *Opt. Lett.* , vol. 29, pp. 1129–1131, 2004.

[6] G.-H. Lee, Z. Jiang, S. Xiao, and A. M. Weiner, "1700 ps/nm tunable dispersion compensation for 10 Gbit/s RZ lightwave transmission," *Electron. Lett.*, vol. 42, pp. 768–770, 2006.

[7] M. Akbulut, A. M. Weiner, and P. J. Miller, "Broadband all-order polarization mode dispersion compensation using liquid-crystal modulator arrays," *J. Lightw. Technol.*, vol. 24, no. 1, pp. 251–261, Jan. 2006.

[8] A. M. Weiner, "Femtosecond pulse shaping using spatial light modulators," *Rev. Sci. Instr.*, vol. 71, pp. 1929–1960, 2000.

[9] M. Shirasaki, "Large angular dispersion by a virtually imaged phased array and its application to a wavelength demultiplexer," *Opt. Lett.*, vol. 21, pp. 366–368, 1996.

[10] S. Xiao, A. M. Weiner, and C. Lin, "Experimental and theoretical study of hyperfine WDM demultiplexer performance using virtually imaged phased-array (VIPA)," *J. Lightw. Technol.*, vol. 23, no. 3, pp. 1456–1467, Mar. 2005.